Title: Myosin driven Actin Filament Sliding is Responsible for Endoplasmic Reticulum and Golgi Movement

Authors: Joseph F McKenna[1*], Stephen E D Webb[2,3], Verena Kriechbaumer[1] and Chris Hawes[1*]

[1]. Plant Cell Biology, Dept. Biological and Medical Sciences, Oxford Brookes University, Oxford, OX3 0BP

[2]. Central Laser Facility, Research Complex at Harwell, Science and Technology Facilities Council, Rutherford Appleton Laboratories, Oxfordshire OX11 0QX

[3]. Present address; Biotechnology and Biological Sciences Research Council, Polaris House, Swindon, SN2 1UH

*Authors for correspondence. Correspondence: chawes@brookes.ac.uk and josephmckenna@brookes.ac.uk

chawes@brookes.ac.uk, ORCID ID 0000-0003-4856-7690
josephmckenna@brookes.ac.uk, ORCID ID 0000-0003-4838-6048
Stephen.webb@bbsrc.ac.uk, ORCID ID 0000-0002-6304-1702
vkriechbaumer@brookes.ac.uk, ORCID ID 0000-0003-3782-5834

Summary

In plants, the actin cytoskeleton and myosins are fundamental for normal dynamics of the endomembrane system and cytoplasmic streaming. We demonstrate that this is in part due to myosin driven sliding of actin filaments within a bundle. This generates, at least in part, the motive force required for cell dynamics *in planta*.

Keywords

Actin, Myosin, Endoplasmic Reticulum, Golgi, FRAP, Photoactivation

Abstract

The plant secretory pathway is responsible for the production of the majority of proteins and carbohydrates consumed on the planet. The early secretory pathway is composed of Golgi bodies and the endoplasmic reticulum (ER) and is highly mobile in plants with rapid remodelling of the ER network. The dynamics of the ER and Golgi bodies is driven by the actin cytoskeleton and myosin motor proteins play a key role in this. However, exactly how myosin motor proteins drive remodelling in plants is currently a contentious issue. Here, using a combination of live cell microscopy and over-expression of non-functional myosins we demonstrate that myosin motor proteins drive actin filament sliding and subsequently the dynamics of the secretory pathway.

Introduction

Many organelles in plant cells display dynamic movements in the cytoplasm. At its simplest these can be divided into two classes. Firstly, classic cytoplasmic streaming, where movement is due to shear forces induced by actomyosin driving larger organelles [1]. This can be particularly apparent in *trans*-vacuolar strands of leaves. Secondly, more controlled movement of organelles over the actin cytoskeleton at the cortex of cells, especially in highly vacuolated tissues [2]. Even before the advent of live cell imaging based on fluorescent protein technology, it had been shown that in plants the endoplasmic reticulum (ER) network structure and Golgi body dynamics are somehow organised by the actin cytoskeleton [3,4]. By the combination of GFP expression and live cell imaging this organisation is exemplified by the movement of Golgi bodies and ER exit sites (ERES) with the ER network [2,5] and the various different movements of the ER, with four distinct forms having been identified [6–9]. Given that the ER and secretory pathway are the primary site of protein and carbohydrate production in plants, and hence the basis of global food supply, understanding the mechanism behind ER remodelling could have wide reaching implications. Both remodelling of the ER and Golgi movement are abolished by depolymerisation of actin, demonstrating the importance of the actin cytoskeleton in intracellular movement [2,7]. In addition, the cortical actin cytoskeleton supports organelle movement and is dynamic in its own right. Actin filaments and bundles continually remodel in the cytoplasm, and this can involve lateral-filament migration, sliding on actin bundles, filament severing and elongation [10–12].

Plants have two classes of myosins, VIII and XI. There are four members of the myosin VIII family, which most likely function as tensors at the cell surface rather than as motors [13]. In arabidopsis there are thirteen members of the myosin XI family most of which display some form of motor activity [14]. The fastest known myosin of *Chara corallina* reaches speeds of up to 50µms^{-1} in *in vitro* assays and is significantly faster than mammalian homologues [15,16]. In higher plant cells, myosin XI motility is up to 5µms^{-1}, an order of magnitude lower than in algae but still 10-fold faster than the closest human homologue (myosin Va [17,18]). Mutant knock-out analysis of four members of the arabidopsis XI family (*xi-k, xi-1, xi2* and *xi-i*) demonstrate that these proteins are important for normal whole-organism and cellular growth as well as Golgi body dynamics [19]. They are also important for normal dynamics of the actin cytoskeleton *in planta*, with the knockout plants showing decreased turnover with a 2-fold reduced filament severing frequency [20]. Chimeric expression of a slow myosin XI-2, composed of the native myosin XI-2 with the motor domain replaced with *Homo sapiens* myosin Vb motor domain or a fast chimeric myosin protein which contains the *Chara corallina* myosin XI motor domain, results in smaller and larger cell size respectively [21]. This correlation between myosin motility and cell size demonstrates the importance of the actomyosin system in plants and its role in biomass production. Over-expression of truncated forms of the myosin XI family in tobacco leaf cells, show that a number of these will inhibit both Golgi and ER movement, presumably by complexing with the native myosin and rendering it non-functional. This could be in a similar manner to mammalian Myosin Va tail domain expression which turns Myosin Va into an inactive conformation [22].

A possible explanation for myosin generated movement is that myosin molecules link the organelles to the actin cytoskeleton and generate the necessary motive force to explain all the observed movements. However, despite a number of publications expressing fluorescently tagged myosin constructs of various different forms, there is no convincing evidence of any full length myosins decorating the ER surface or Golgi bodies [14,23]. It has however been suggested that myosin XI-K associates with endomembrane-derived vesicles in arabidopsis [24]. DIL domain (homologue of a yeast secretory vesicle binding domain of Myo2p) constructs from arabidopsis myosin XIs locate to various organelles and only one from myosin XI-G labels Golgi and ER [25]. Thus, apart from these few hints, it is still an open question as to how force is generated to induce motility in the two major organelles of the secretory pathway, the ER and Golgi bodies in conjunction with the actin cytoskeleton.

A possible mechanism to explain movements of the cortical ER network is that the motive force comes from motile Golgi bodies attached to the actin cytoskeleton [26]. Golgi bodies associated with ER networks are restricted to curved membrane surfaces in yeast [27] and higher plants [28]. It was demonstrated in tobacco leaf cells that if Golgi bodies were disrupted with Brefeldin A, resulting in the reabsorption of Golgi membrane back to the ER, ER motility still persisted [4]. It is however possible that a residual matrix of Golgi associated proteins and putative ER tethers remains after such experiments and could still remain associated with the actin cytoskeleton during such drug treatments [29,30].

Direct contacts between ER and actin have been reported [31,32]. Cao et al., (2016) [32] reported that the SNARE protein SYP73 may act as a linker between the ER, myosin and the actin cytoskeleton. Although an earlier report of the closely related ER SNARE SYP72 suggested that its function was to mark Golgi-ER import sites on the surface of the ER

membrane, with no mention of any association with actin or actin binding proteins [33]. Likewise a protein of the NETWORKED family, NET 3B has been shown to bridge between the ER and actin bundles [34].

Another explanation for some of the observed ER/Golgi motility is that there is no direct connection between actin filaments, myosin and the organelles, even via linker or receptor proteins. Here we have used three different probes for plant actin, fABD2 [10,35] Lifeact [36,37] and a GFP tagged anti-actin alpaca nanobody [38] which, when expressed, self-immunolabels the actin cytoskeleton. We demonstrate that upon overexpression of a dominant negative myosin tail domain, Fluorescence Recovery After Photobleaching (FRAP) of all three actin marker labels is reduced. Furthermore, upon photoactivation of actin labelled lines, the signal migrates out of the activation area to adjacent actin filaments, and this is inhibited by overexpression of the dominant negative myosin tail domain. Our hypothesis is that ER remodelling is generated by myosin induced sliding of actin filaments over one another and that a non-motor link between actin filaments and ER membrane most likely transfers motive force to the ER membrane, perhaps via SNAREs or NET proteins such as SYP73 and NET3B [32,34].

Results

ER tubule elongation moves over existing actin bundles

The cortical ER in cotyledon and mature leaf epidermal cells shows various differing movements including polygon rearrangement, movement of the membrane surface and tubule outgrowths [7]. To test if the latter was mediated by actin filament polymerisation, we transiently co-expressed GFP-fABD2 with the ER marker ssRFP-HDEL and imaged with sub-diffraction-limited resolution using the Airyscan detector (Fig. 1; video 1). We found no evidence of ER tubules tracking actin filament polymerisation. However, growing tubules were routinely imaged moving along pre-existing actin bundles (Fig. 1 and video 1, white arrows).

FRAP recovery of labelled actin cytoskeleton demonstrates myosin dependence

We have previously shown that expression of non-functional myosin XI tail fragments can inhibit movement of Golgi bodies and the ER [26,39]. However, fragments from several of the 13 myosin XI isoforms, on expression in tobacco leaf cells, had no or negligible effects on endomembrane dynamics. We therefore combined our experiments with transient expression of myosin tail fragments in benthamiana leaf pavement cells, to assess the potential role of myosins in actin filament sliding within actin bundles. We decided not to use myosin inhibitor drugs such as BDM or ML-7 as their specificity in plants has been called into question [40,41]. Initially we used Total Internal Reflection Fluorescence (TIRF) microscopy to image actin filaments and bundles with high temporal and spatial resolution. In addition to the previously reported changes in actin cytoskeleton structure in myosin knockout mutant lines [1], actin filament dynamics were also impaired (Fig. 2A&B) when a dominant negative myosin tail domain (XI-K) was overexpressed (Fig.2A&B). Reductions in actin dynamics and more bundled networks have previously been reported for triple knockout mutants in arabidopsis [1,20]. Here we demonstrate that this is phenocopied in *N. benthamiana* with

transient expression of a dominant negative myosin tail domain (Fig. 2). In order to determine in more detail how fluorescence recovery occurs, we performed FRAP experiments by TIRF microscopy. This recovery occurs along existing filaments (Fig. 2C), but not uniformly, as one would expect if recovery was due to new binding of GFP-fABD2 along the entire length of the filament. For actin labelled with fABD2-GFP and imaged using confocal microscopy, recovery after photobleaching was significantly impeded when myosin XI-K tail fragments were transiently expressed in the leaves (Fig. 3A-D; video 2). Control plateau and $t_{1/2}$ values were 59.55 ± 17.7% (SD) and 4.6 ± 2s (SD) compared to XI-K values of 44.4 ± 17.6% (SD) and 6.1 ± 3.2s (SD) respectively (Fig. 3B-D) ($p \leq 0.0001$ for plateau, $P \leq 0.001$ for $t_{1/2}$, ANOVA). On expression of a tail fragment of myosin XI-A, previously shown not to inhibit mitochondria movement [39] or ER remodelling [42], there was no significant effect on fluorescence recovery. Therefore, the observed effects with XI-K are not due to unspecific expression of tail domains, but only those which inhibit endomembrane dynamics (XI-K). This suggests that myosins contribute toward the recovery of labelled actin fluorescence by supporting inter-filament actin sliding. Photobleaching was also performed on the reporter GFP-Lifeact in combination with XI-K tail domain expression (Supplementary Fig. S1B-E) and the intensity plateau level was significantly reduced between the control and XI-K, and between XI-A and XI-K (Fig. S1). The $t_{1/2}$ values for Lifeact photobleaching were not significantly different between the control and, XI-K or XI-A. To summarise, in two different actin marker lines, expression of the inhibitory tail domain of XI-K reduced actin dynamics.

Similar experiments were carried out on the actin cytoskeleton in cotyledon epidermal cells self-immunolabelled by transient expression of an alpaca chromobody against actin [38] and tagged with GFP (Fig. 3E-G and S1A, GFP-actinCB). Inhibition of fluorescence recovery after bleaching in the presence of myosin XI-K was not as dramatic as with fABD2-GFP labelled actin but still significant (Fig. 3F&G). Plateau values were 70.9 ± 8.5% (SD) for the control and 62 ± 18.5% (SD) for XI-K, a statistically significant difference ($p \leq 0.0001$, ANOVA, Fig 1B and C). The $t_{1/2}$ values were 1.8 ± 0.8s (SD) for control and 2.4 ± 2.3s (SD) for XI-K, also a statistically significant difference ($p \leq 0.05$, ANOVA, Fig. 1D).

Actin labelled FRAP recovery is not due to actin polymerisation.

As a further control we measured fluorescence recovery of actin bundles after treatment with jasplakinolide which has previously been used *in planta* to stabilise actin filaments [43,44]. It induces hyper actin polymerisation, resulting in the depletion of available G-actin in the cell and therefore inhibiting subsequent polymerisation [45,46]. Jasplakinolide treatment did not significantly alter the recovery period, plateau or $t_{1/2}$ of GFP-fABD2 labelled actin filament bundles (Fig 4A-D). This indicates that recovery was not due to actin filament polymerisation into the bleached zone. This was the same for the GFP-actinCB after jasplakinolide treatment (Supplementary Fig. S2), with no statistically significant difference in plateau level or $t_{1/2}$. However, there was a significant decrease in Golgi velocity on treatment with the drug (Fig. 4E), although at this stage we have no information as to whether this reflects on a secondary effect of the treatment.

Photoactivation demonstrates myosin dependant sliding of actin filaments.

207 Alongside the photobleaching experiments, we confirmed our results by transiently
208 expressing fABD2 or Lifeact linked to mCherry and photoactivatable-GFP (paGFP). In this way,
209 it was possible to quantify the dispersal of the activated GFP along actin filaments (Fig.5A-E,
210 arrows; video 3). On activation of the mCherry-paGFP constructs, the green fluorescence
211 signal rapidly dispersed laterally over the mCherry labelled filaments (Fig. 5A; video 3).
212 Measuring the intensity increase of an adjacent ROI a set distance from the activated region,
213 an increase in GFP fluorescence occurred above the initial activation level after timepoint 0s
214 (Fig. 5B). Both the plateau value and $t_{1/2}$ of the activated ROI are significantly higher when
215 expressed with XI-K than in the control or XI-A (control plateau: 5.9 ± 5.7% (SD), XI-K plateau
216 11.3 ± 13.4% (SD), Fig. 5D, control $t^{1/2}$ 3.1 ± 1.3s (SD), XI-K $t^{1/2}$ 5.1 ± 3.5s (SD), Fig. 5E). XI-A
217 photoactivation was similar to the control, demonstrating the specificity of XI-K expression to
218 filament recovery. In addition, mCherry-paGFP-Lifeact activation showed a slower $t_{1/2}$ when
219 expressed with XI-K than in the control or XI-A condition (Supplementary Fig. S3). Therefore,
220 activated paGFP labelled actin moved more slowly out of the ROI when XI-K was expressed.
221 This further demonstrated that sliding of actin filaments within actin bundles is regulated by
222 myosins.
223
224 **Discussion**
225
226 ***Myosins are responsible for actin filament sliding***
227
228 There are a number of ways in which the actin cytoskeleton can support movement within
229 eukaryotic cells. These include the interaction between myosin motors, organelles and actin
230 filaments; the rapid polymerisation of actin filaments and the myosin-driven sliding of actin
231 filaments over each other within actin bundles. Plant myosins are now well documented and
232 have long been known to support cytoplasmic streaming in a wide range of cells [47].
233 However, regarding the secretory pathway, the role of actin in the dramatic remodelling of
234 the cortical ER network [1,3,7,42] and the movement of individual Golgi stacks [2,48–50] has
235 been the subject of a number of reports. It has also been noted that Golgi bodies move in
236 concert with the moving bounding membrane of the ER [6,51]. Although it is clear that
237 members of the myosin XI family are involved in such movements [14,39,42,52], there is no
238 convincing evidence for direct endomembrane organelle-myosin-actin interactions, with the
239 exception that myosin XI-K constructs potentially labelling some post-Golgi compartments in
240 roots. It was also suggested XI-K labelled ER derived vesicles in leaves with some ER labelling
241 [24]. Furthermore, in a quadruple myosin mutant knockout line, the actin cytoskeleton
242 structure is altered in addition to organelle dynamics [19]. Additionally, fluorescently tagged,
243 myosin XI-K labels the actin cytoskeleton preferentially to post-Golgi compartments, as
244 determined by co-localisation [19].
245
246 Here we demonstrate that new ER tubule formation occurs predominantly along existing actin
247 bundles (Fig. 1). This demonstrates that either myosins moving along existing actin filaments
248 or inter-filament sliding of actin dragging newly forming ER tubules occurs. We then used
249 photobleaching and photoactivation to determine if myosin driven actin filament sliding
250 occurs. The interpretation of fluorescence recovery data from fluorescent protein-tagged
251 actin networks in plants can be fraught with problems. Both the commonly used fABD2 and
252 Lifeact constructs bind to actin filaments and are subject to on and off turnover on the
253 filaments themselves [53]. Thus, data from bleaching experiments can either be interpreted

as a measurement of turnover of the actin binding fragments or movement/recovery of the actin filaments/bundles themselves. To mitigate this problem, we also utilised actin labelling by the expression of a cameloid actin nanobody spliced to GFP. This results in self-immunolabelling *in vivo* of the actin network [38]. Being an antibody fragment, its turnover rate on the actin filaments is very low. The results obtained were the same as those with the classic actin markers Lifeact and fABD2, demonstrating that myosin perturbation affects the recovery of fluorescence of the labelled actin cytoskeleton. This further supports the hypothesis that myosin drives filament sliding within actin bundles. Over-expression of a non-inhibiting XI-A myosin tail fragment had no effect on FRAP recovery of the actin labels used, therefore the results obtained are specific to ER and Golgi regulating myosins.

Jasplakinolide stabilises the actin cytoskeleton and depletes the pool of G-actin thereby not allowing subsequent polymerisation. After jasplakinolide treatment, we did not see an effect on photobleaching recovery of fluorescently labelled actin (Fig. 4), which is further proof that the recovery we observed is due to myosin driven filament sliding and not polymerisation. Furthermore, while there is a reduction in Golgi body velocity after jasplakinolide treatment, they are still moving and the actin network structure is perturbed. The decrease in movement could be due to network structure changes. As cytoskeleton FRAP recovery still occurs and Golgi bodies are still mobile this implies that myosin driven filament sliding contributes to their mobility and hence ER remodelling.

In parallel, we also employed photoactivatable constructs to label the cortical actin cytoskeleton, which report on the movement of activated fluorescence *and* the actin network simultaneously, not simply the turnover of constructs on the filaments. This photoactivation strategy clearly demonstrates movement of fluorescence (and hence bound actin) out of the activated regions into adjacent ones along existing actin filaments. This clearly demonstrates actin filament sliding. Furthermore, upon co-expression with a dominant negative myosin-tail domain, the loss of paGFP fluorescence out of the activation region is reduced, demonstrating that the filament sliding observed is, at least in part, myosin dependant.

Summary.

Utilising the photobleaching and activation strategy our results demonstrate that the cortical actin filaments within bundles are sliding over each other powered by one or more myosins. To support movement of the ER and Golgi bodies attached to it, it would be necessary to anchor the ER membrane to underlying actin filament bundles. Several recent reports have suggested that SNARE proteins (SYP 73, [32]) and members of the NETWORKED family, NET3b over the ER [34] and NET3c at ER-plasma membrane contact sites [54], may perform this role. Myosin regulation of actin network structure has been reported previously, with the mammalian myoX motor function being critical for actin reorganisation at leading edges, resulting in filopodia formation [55]. In addition, the mammalian myosin1c stabilises ER sheets via regulation of actin filament array organisation [56]. Furthermore, it has been demonstrated *in planta* that myosins are responsible for generating the force required for buckling and straightening of both individual filaments and bundles [20]. Elegant work using optical tweezers has also demonstrated a role for myosin in actin entry into generated cytoplasmic protrusions [57]. Both of these *in planta* observations hypothesized that myosin facilitated sliding of filaments could account for this, which our work demonstrates.

We propose a new model that both ER and Golgi movement are, at least in part, a result of myosin driven sliding of actin filaments within actin bundles that underlie and are anchored to the ER (Fig. 6). This model can account for differences in speeds of ER and Golgi movement. Myosin motors and actin filaments can act independently or synergistically with each other to induce a range of different speeds of sliding, resulting in differential movement of the filaments attached to the ER. Indeed this model could also explain the differences in cell size observed when expressing fast and slow chimeric myosins [21] as these would result in respectively increased and reduced filament sliding and cytoplasmic streaming, hence larger and smaller cells. It can also explain the perturbed actin cytoskeleton observed in triple and quadruple mutant knockout lines. Furthermore, if there are different polarities of actin filaments within a bundle then directionality of ER membrane and associated organelle movement can be controlled in this manner.

Acknowledgements

We thank Dr Mark Fricker for helpful discussions and Dr Frances Tolmie for useful comments on the manuscript. We thank the Oxford Brookes Bioimaging unit for financial support. Access to the TIRF iLas system was provided under an STFC facility access grant to JM and SW (16230034).

Author contributions

JM and CH conceived the experiments and wrote the manuscript. CH secured funding. JM and SEDW performed the experiments. VK provided genetic resources. All authors reviewed and edited the manuscript.

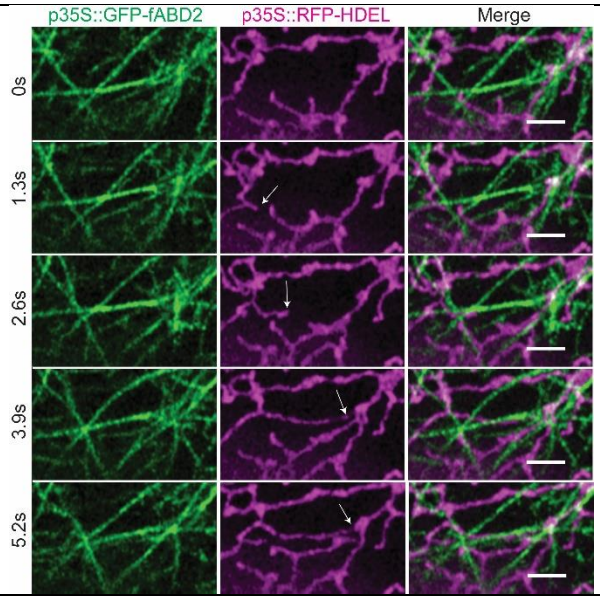

Figure 1. Airyscan imaging of an endoplasmic reticulum tubule elongating over existing actin filaments in *N. benthamiana*. N = 60 cells across 3 experimental repeats. Representative images shown. White arrows showing growing ER tubule. Scale bar = 2µm.

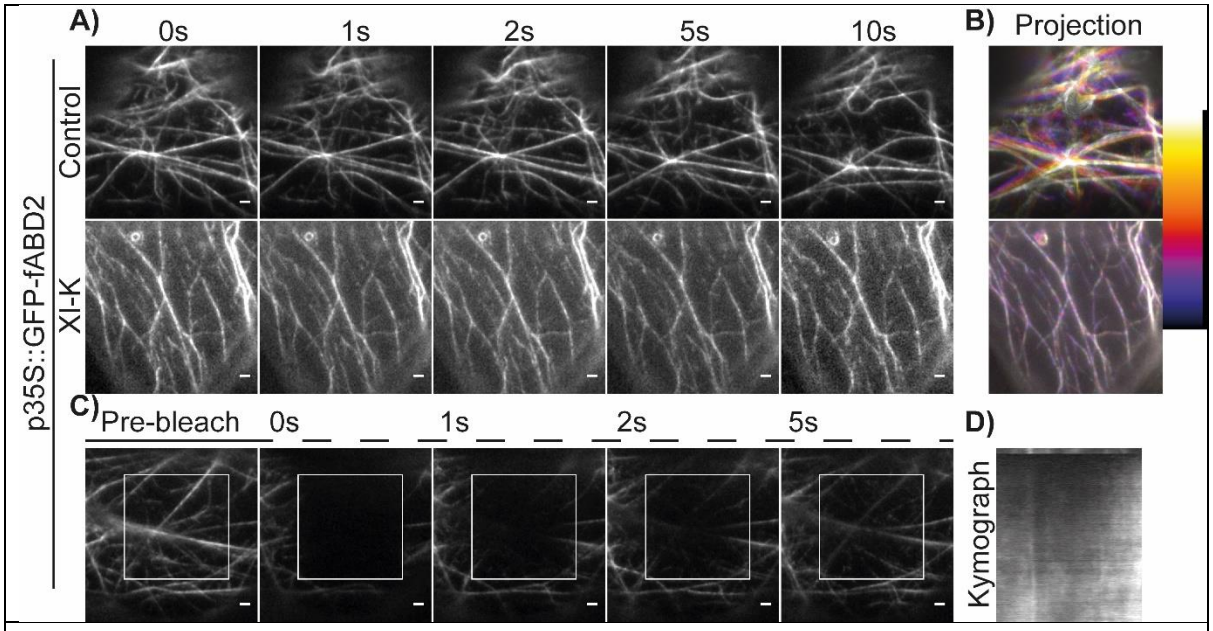

Figure 2. TIRF imaging and transient expression in *N. benthamiana* demonstrates dominant negative myosin XI-K tail domain perturbs actin dynamics *in planta*. A) TIRF Time course data from labelled GFP-fABD2 control and with p35S::RFP-XI-K. N=20 cells, representative images shown. B) Temporal colour coded projection of time-course data in A). C) Fluorescence recovery from the actin cytoskeleton labelled with GFP-fABD2 occurs along existing filaments. N=30 cells, representative images shown. D) Kymograph showing FRAP recovery along actin filament occurs from either side of the bleach region. Scale bar = 2µm.

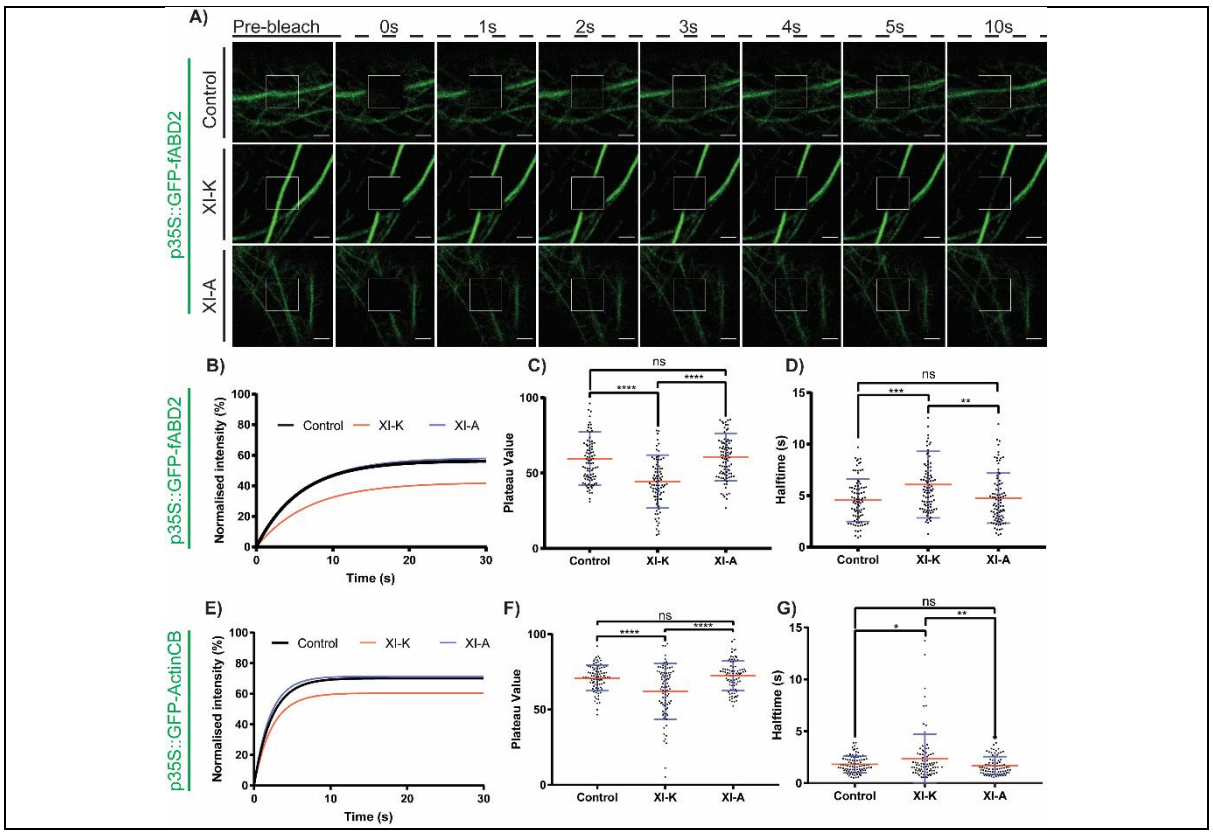

Figure 3) Inhibition of myosin via overexpression of a dominant negative tail domain reduces GFP-fABD2 labelled actin FRAP recovery in *N. benthamiana*. A) Time-course of confocal FRAP showing fluorescence recovery of GFP-fABD2 and co-expression with the dominant negative p35S::RFP-XI-K tail domain. The XI-A tail domain had no effect on ER remodelling or Golgi mobility and so was used as a negative control. B) Fluorescence recovery curves, C) plateau values, D) halftimes of fluorescence recovery for GFP-fABD2 FRAP from control, XI-K and XI-A treatment. E) Fluorescence recovery curves, F) plateau values, G) halftimes of fluorescence recovery for GFP-actinCB FRAP from control, XI-K and XI-A treatment. For boxplots, error bars (blue) denote standard deviation, mean value (red) is shown. ANOVA statistical analysis was performed. ns = p≥0.05, **=p≤0.01, ***=p≤0.001, ****=p≤0.0001. N=90 cells, across 3 experimental repeats. Scale bar = 2µm.

331

332

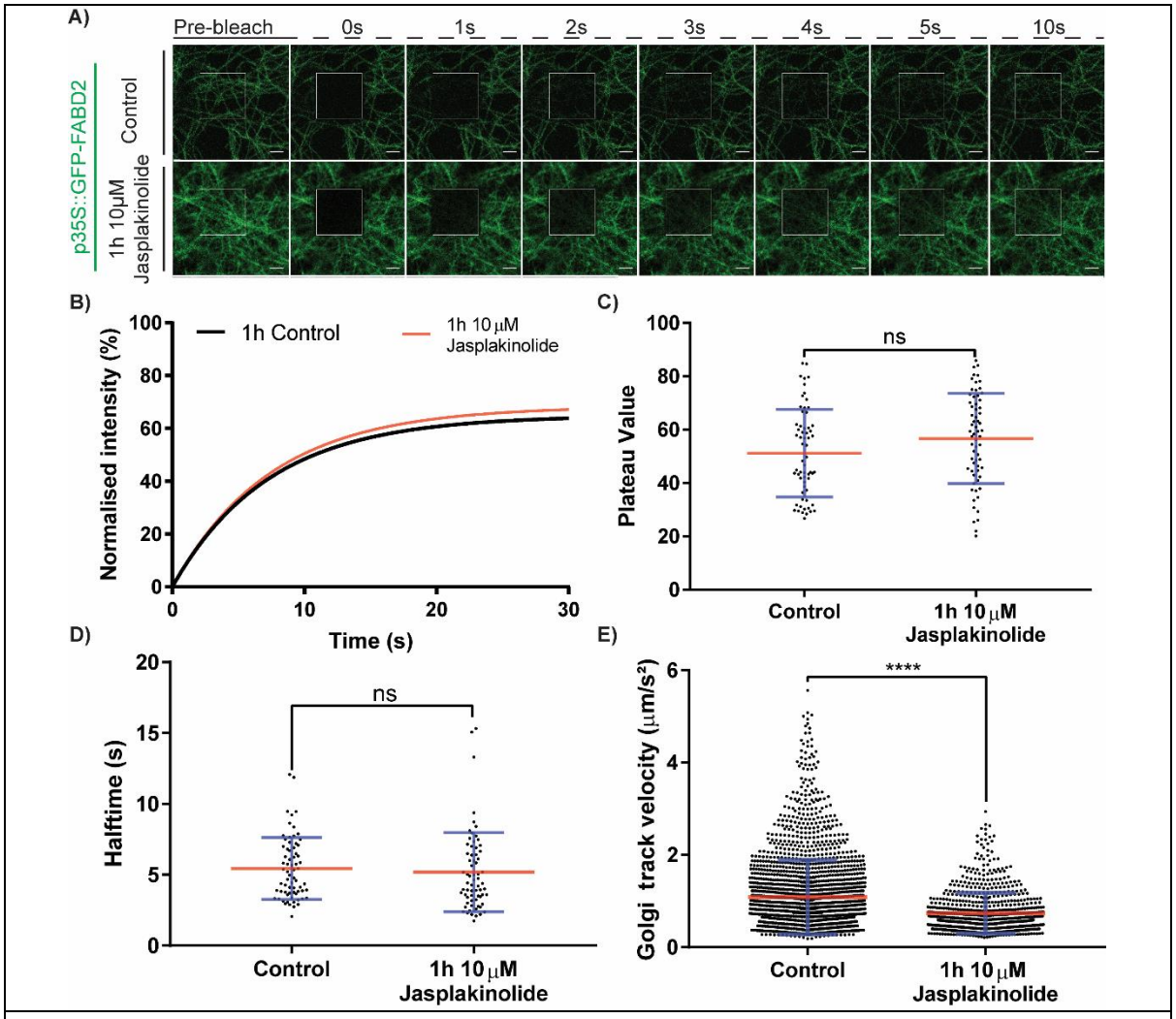

Figure 4. Treatment with Jasplakinolide and stabilisation of actin does not affect FRAP but does affect Golgi body mobility in *N. benthamiana*. A) Time-course of fluorescence recovery of GFP-fABD2 after Jasplakinolide treatment. N=≥63 cells across 3 experimental repeats per condition. B) Fluorescence recovery curves, C) plateau values and D) half-times of fluorescence recovery for control and 1h 10µM Jasplakinolide treated GFP-fABD2. E) Golgi track velocity of p35S::ST-RFP labelled Golgi bodies in 1h control and 10µM Jasplakinolide treated tissue. N=30 cells per condition. All experiments performed

with transient infiltration in *N. benthamiana*. For boxplots, error bars (blue) denote standard deviation, mean value (red) is shown. Student T-test statistical analysis performed. ns = p≥0.05. ****=p≤0.0001. Scale bar = 2µm.

333

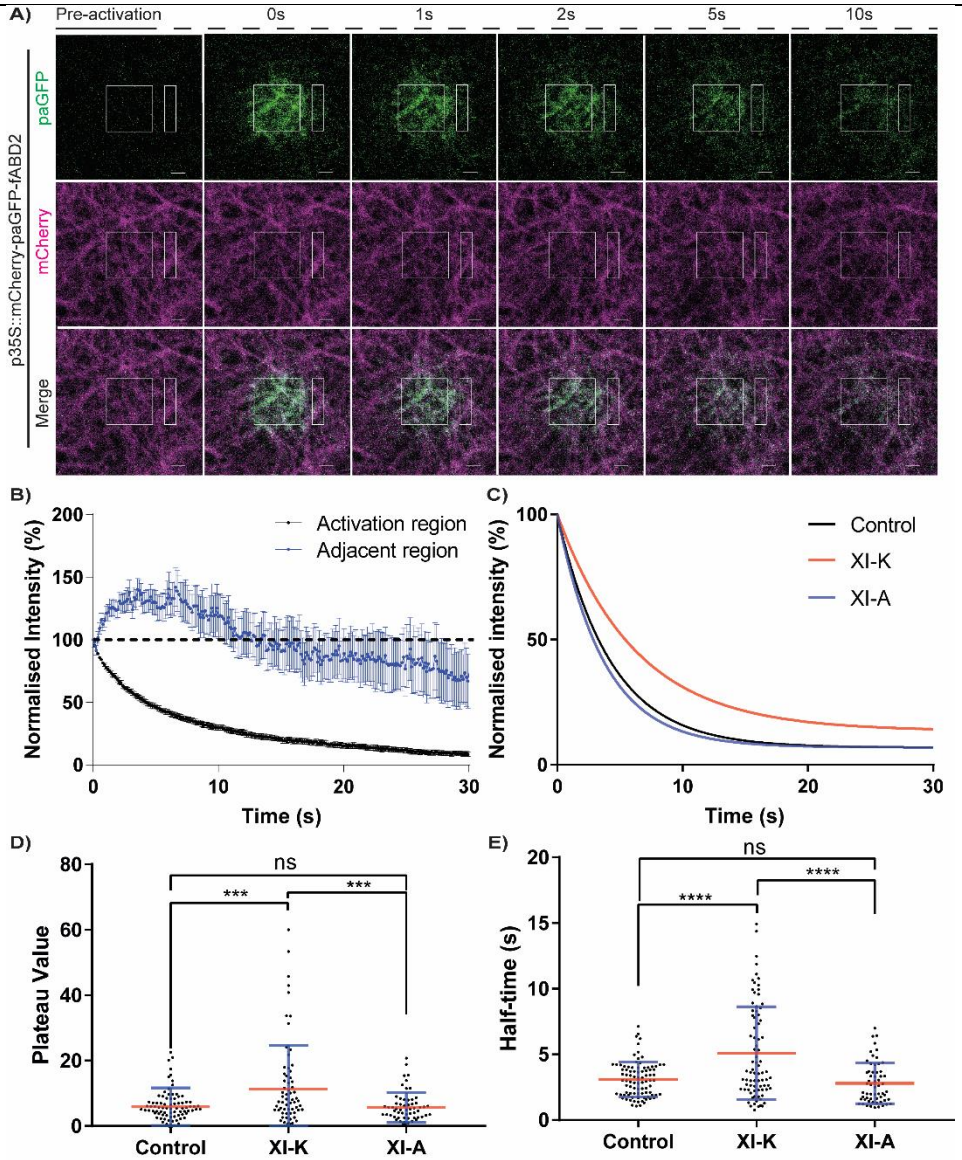

Figure 5. Photoactivation of dual labelled fABD2 lines demonstrates filament sliding is driven by myosins in *N. benthamiana*. A) Time- course of activation in control data. Activated region (central square) and adjacent non-activated region (white rectangle) are shown. mCherry (magenta) and paGFP (green) channels shown. B) Normalised intensity curve for activation region (black) and adjacent region (blue) (error bars = SE). C) One phase-decay plot for control, XI-K and XI-A expressing cells labelled with the dual marker. D) Plateau value from one-phase decay plot (C). E) Half-time of photoactivated actin marker. For boxplots, error bars (blue) denote standard deviation, mean value (red) is shown. ANOVA statistical analysis was performed. ns = p≥0.05, ***=p≤0.001, ****=p≤0.0001. N=≥60 across 3 experimental repeats. Scale bar = 2µm.

334

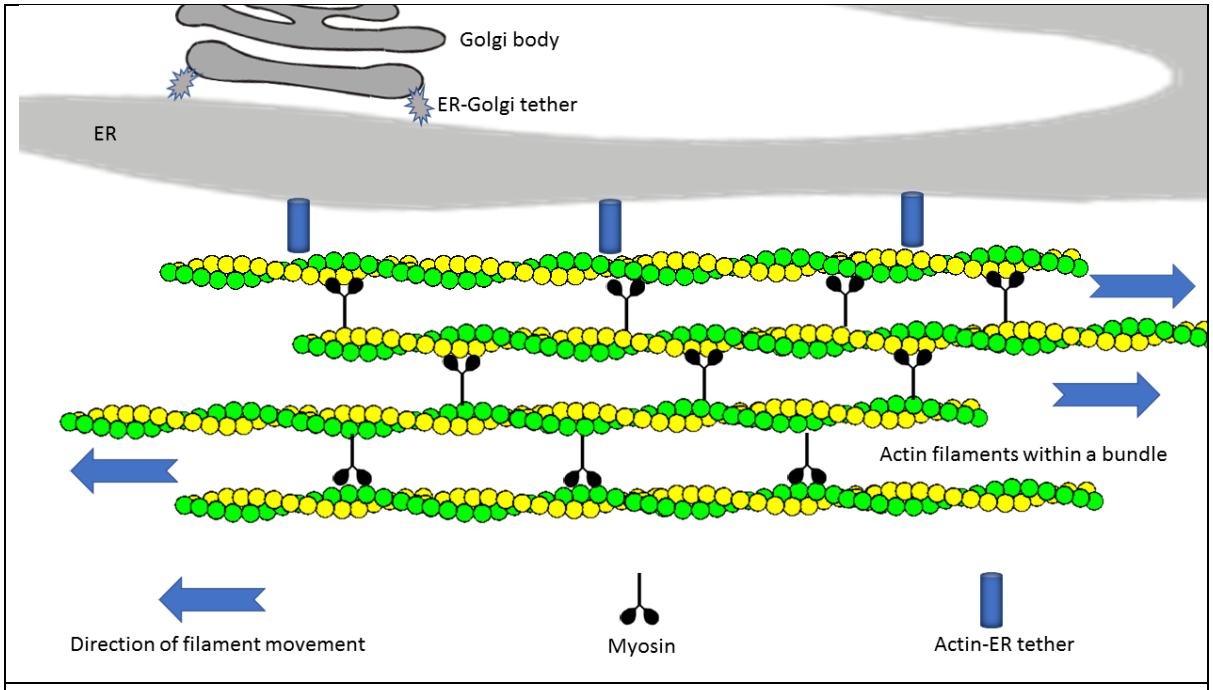

Figure 6. A model showing how myosin driven actin sliding with the combination of tethering proteins can potentially drive ER and Golgi mobility. Myosins are shown linking actin filaments within a bundle and are responsible for filament sliding. Potential linker proteins (such as SYP73) are shown tethering the ER to the actin cytoskeleton [32]. The Golgi bodies are tethered to the ER [50] and hence the physical force generated by actin sliding accounts for ER remodelling and Golgi body movement.

335
336

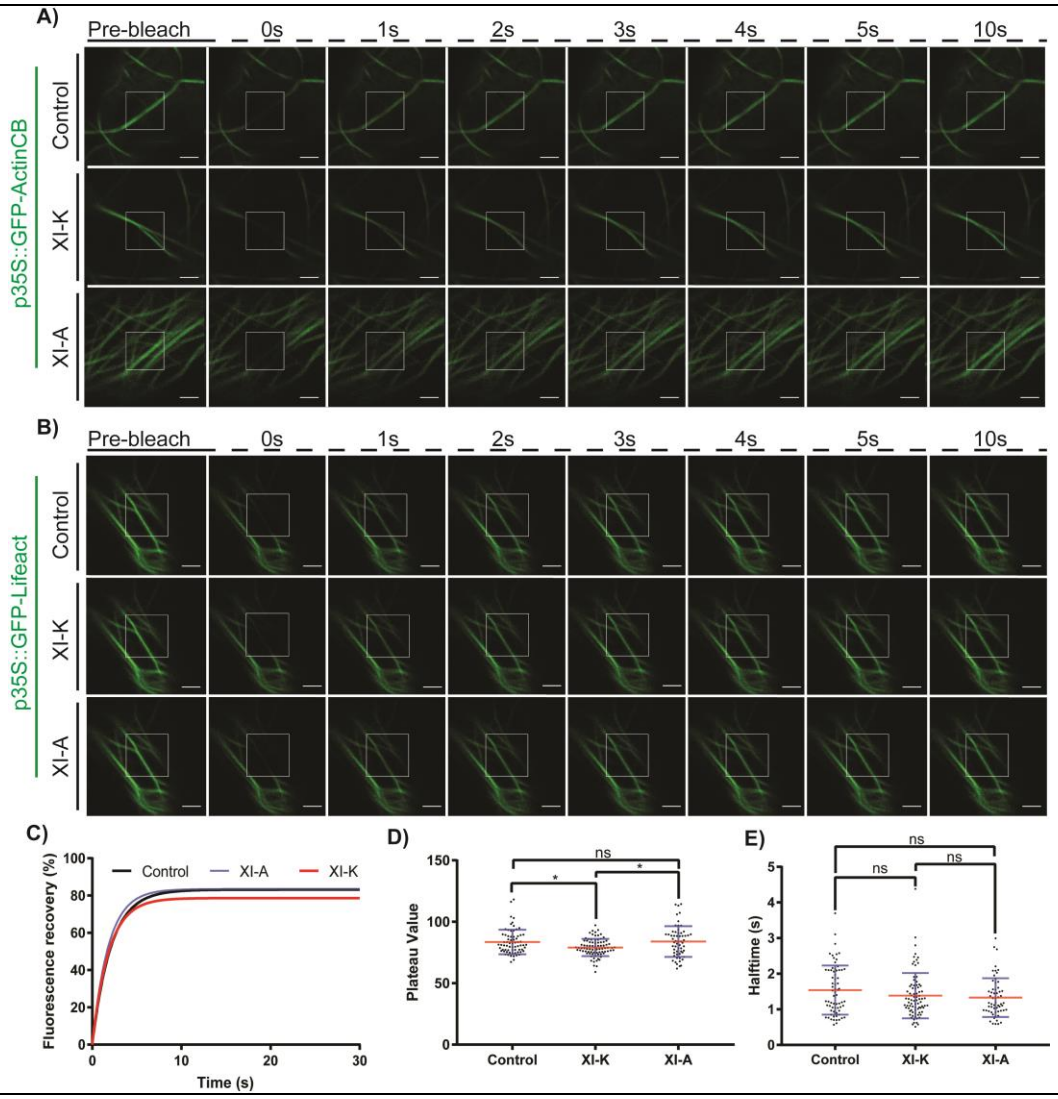

Supplemental Figure 1. GFP-ActinCB and GFP-Lifeact FRAP with control, XI-K and XI-A expression transiently expressed in *N. benthamiana*. A) FRAP time course of GFP-actinCB labelled actin bundles in control, XI-K and XI-A conditions. FRAP quantification data in Fig. 3. B) FRAP time course of GFP-Lifeact labelled actin bundles in control, XI-K and XI-A conditions. B) Fluorescence recovery curves, C) plateau values and D) $t^{1/2}$ of fluorescence recovery of actin bundles labelled with GFP-Lifeact shown in (A). For boxplots, error bars (blue) denote standard deviation, mean value (red) is shown. ns = p≥0.05, *=p≤0.05, ANOVA. N=≥59 cells, across 3 biological repeats per condition. Scale bar=2µm.

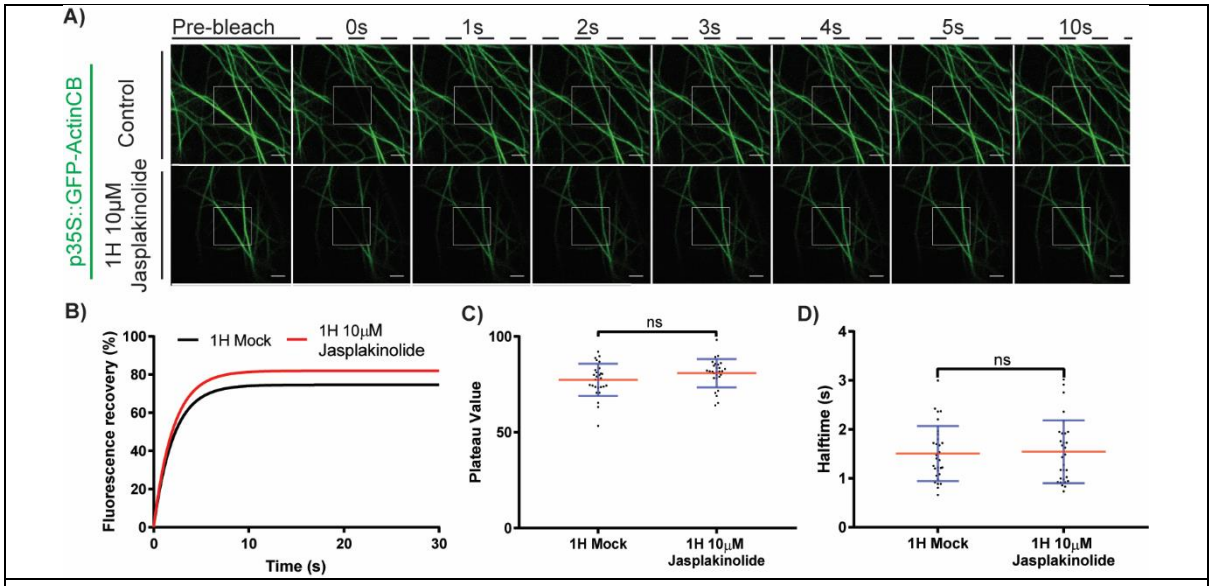

Supplemental Figure 2. GFP-ActinCB FRAP recovery after treatment with jasplakinolide in transiently expressing *N. benthamiana*. A) FRAP time course of GFP-ActinCB labelled actin in 1h control and jasplakinolide treatments. B) Fluorescence recovery curves, C) plateau values and D) $t^{1/2}$ of fluorescence recovery of actin shown in (A). For boxplots, error bars (blue) denote standard deviation, mean value (red) is shown. ns = p≥0.05, Students T-test. N=28 cells per condition.

339

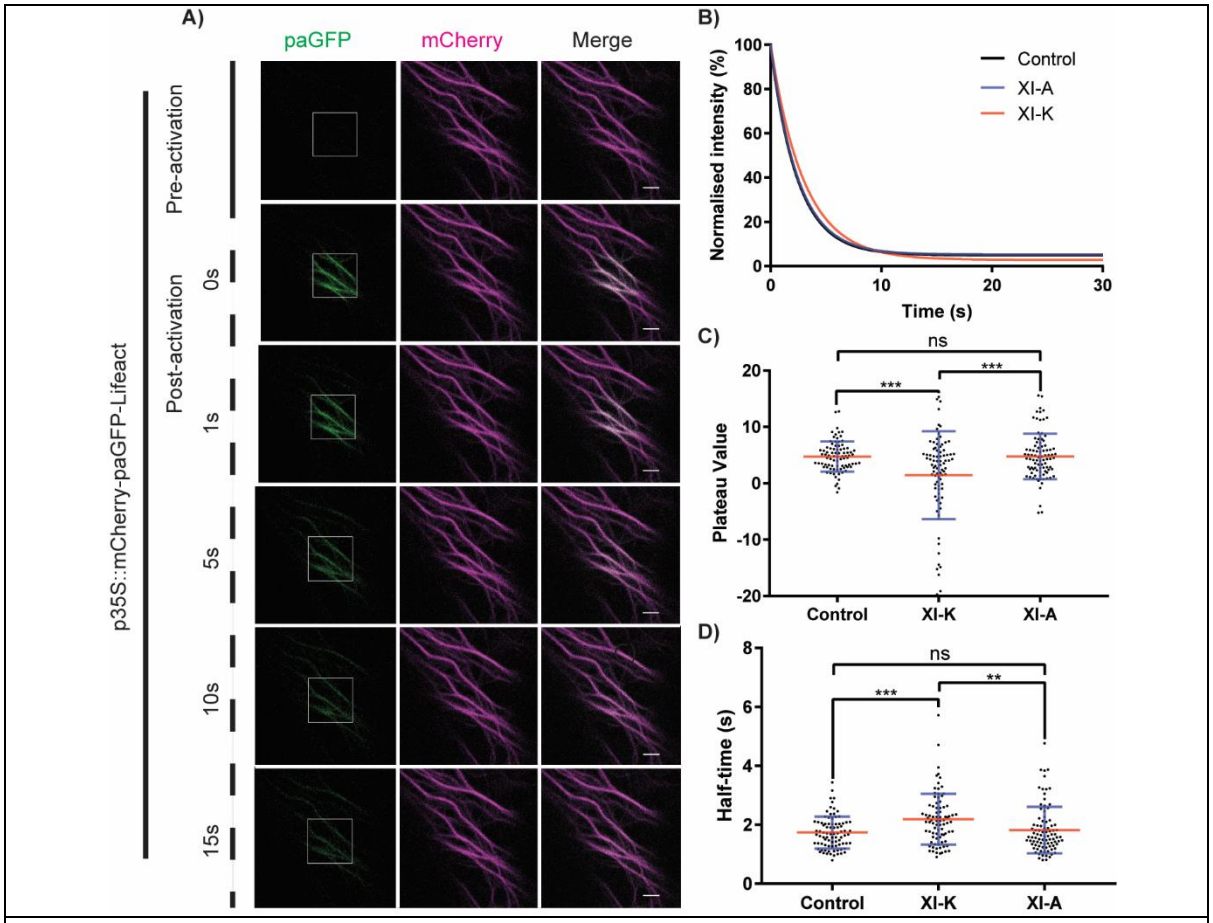

Supplemental Figure 3. Photoactivation of mCherry-paGFP-Lifeact in control, XI-K and XI-A in transiently expressing *N. benthamiana* cells. A) Photoactivation of mCherry-

paGFP-Lifeact labelled actin shows activated GFP sliding over actin filaments. B) Fluorescence decay curves, C) plateau values and D) $t^{1/2}$ of fluorescence decay of control, XI-K and XI-A activated paGFP in (A). For boxplots, error bars (blue) denote standard deviation, mean value (red) is shown. ns = p≥0.05, ** = p≤0.01, *** = p≤0.001, ANOVA multiple comparison test. N=≥68 cells, across 3 experimental repeats per condition.

Supplementary table 1

Primers used in this study:

JM393	GGGGACAAGTTTGTACAAAAAAGCAGGCTcgATGGTGAGCAAGGGCGAGGAG
JM394	acctccactgccaccCTTGTACAGCTCGTCCATGCCG
JM395	GTACAAGggtggcagtggaggtatgGATCCTCTTGAAAGAGCTGAATTGGTTCTC
JM392	GGGGACCACTTTGTACAAGAAAGCtgggtCTATTCGATGGATGCTTCCTCTGAGACC
JM401	GGGGACCACTTTGTACAAGAAAGCtgggtctaTTCTTCCTTTGAGATGCTTTCGAATTT CTTGATCAAATCTGCGACACCCATacctccactgccaccCTTGTAC

Movie 1: Time lapse series of ER tubules (labelled with p35S::RFP-HDEL) elongating over existing actin bundles (labelled with p35S::GFP-fABD2) in *N. benthamiana* transiently expressing leaf epidermal cells. Images same as in Fig. 2. White arrows show tip of elongating tubule. Scale bar denotes 2µm.

Movie 2: Time lapse series showing Flourescence recovery after photobleaching (FRAP) of GFP-fABD2 labelled actin expressed solo and with the myosin tail domains of XI-A or XI-K. Construct expression is transient in *N. benthamiana* leaf epidermal cells. White box indicates bleach region. Images same as in Fig. 4. Scale bar denotes 2µm.

Movie 3: Time lapse series showing photoactivation of paGFP of mCherry-paGFP-fABD2 labelled actin cytoskeleton bundles, demonstrating filament sliding. Construct expression is transient in *N. benthamiana* leaf epidermal cells. White box indicates activation region. Images same as in Fig. 7. Scale bar denotes 2µm.

STAR* Methods

REAGENT or RESOURCE	SOURCE	IDENTIFIER
Bacterial and Virus Strains		
E. Coli strain DH5α	Widely distributed	N/A
A. tumefaciens strain GV3101	Widely distributed	N/A
Chemicals, Peptides, and Recombinant Proteins		
Q5® High-Fidelity DNA Polymerase	NEB	Cat# M0491S
NEBUILDER® HiFi DNA Assembly Master Mix	NEB	Cat# E2621S
MES hydrate	Sigma	Cat# M8250-100G

triSodium orthophosphate (Na_3PO_4)	BDH	Cat# 1777680
Acetosyringone (4'-Hydroxy-3',5'-dimethoxyacetophenone)	Sigma	Cat# D134406
D-Glucose	Fisher	Cat# G/0500/53
Jasplakinolide	Cambridge bioscience	Cat# CAY11705-50ug
Spectinomycin	Melfords	Cat# S23000-25
Rifampicin	Melfords	Cat# R0146
Gentamicin	ThermoFisher	Cat# 15710-049
BP Clonase	Invitrogen	Cat# 56480
LR Clonase	Invitrogen	Cat# 56485
Critical Commercial Assays		
Nucleospin®-plasmid	Macherey-Nagel	Cat# 740588.250
Nucleospin®- Gel and PCR cleanup	Macherey-Nagel	Cat# 740609.250
Experimental Models: Organisms/Strains		
N. benthamiana	Widely available	N/A
A. tumefaciens strain GV3101 p35S::RFP-XI-A	[39]	N/A
A. tumefaciens strain GV3101 p35S::RFP-XI-K	[39]	N/A
A. tumefaciens strain GV3101 p35S::GFP-fABD2	[10]	N/A
A. tumefaciens strain GV3101 p35S::GFP-Lifeact	[35,37]	N/A
A. tumefaciens strain GV3101 p35S::GFP-ActinCB	This study	N/A
A. tumefaciens strain GV3101 p35S::mCherry-paGFP-fABD2	This study	N/A
A. tumefaciens strain GV3101 p35S::mCherry-paGFP-Lifeact	This study	N/A
Oligonucleotides		
A list of oligonucleotides is given in Table S1		
Recombinant DNA		
pDONR221	Invitrogen	Cat# 35-1687
pB7WGF2	VIB, Gent	N/A
pB7WGC2-mCherry	Modified from VIB, Gent, provided by John Runions, Oxford Brookes university.	
p35S::GFP-ActinCB	This study	Modified from Chromotek ActinCB® https://www.chromotek.com/products/chromobodies/actin-chromobodyr/actin-chromobodyr-plasmid/
p35S::mCherry-paGFP-fABD2	This study	N/A
p35S::mCherry-paGFP-Lifeact	This study	N/A
Software and Algorithms		
Fiji	https://fiji.sc/	v1.52h

Zeiss Zen Black	https://www.zeiss.com/microscopy/int/products/microscope-software/zen-lite.html	v2.1 SP3 14.0.0.0.
Zeiss Zen Blue	https://www.zeiss.com/microscopy/int/products/microscope-software/zen-lite.html	v2.3
Graphpad	https://www.graphpad.com/scientific-software/prism/	v7.04
Adobe illustrator CC	https://www.adobe.com/uk/products/illustrator.html	v22.0.1

Experimental model and subject details

Plant lines used and chemical treatments

N. benthamiana transient transformation was performed as described in Sparkes et al., [58]. All fluorophore-labelled marker lines were infiltrated with an *Agrobacterium* optical density at 600nm (OD) of 0.05. p35S::RFP-XI-A and p35S::RFP-XI-K [39] were transformed with an OD of 0.01. Imaging was performed at 3 days post infiltration (dpi). A Jasplakinolide stock solution (10mM) in DMSO was diluted to a working concentration of 10 µM in dH_2O. Plant samples were incubated for 1h in Jasplakinolide or control (same concentration of DMSO) solutions.

Method details

Cloning constructs.

GFP-ActinCB: The Actin-Chromobody® plasmid containing the alpaca actin-antibody gene was obtained from Chromo-Tek (Martinsried, Germany [38]). Primers were ordered from Eurofins MWG Operon (Ebersberg, Germany). Q5 highfidelity DNA polymerase (New England Biolabs, Herts, UK) was used for the polymerase chain reaction (PCR) reaction. The ActinCb-PCR product was cloned into the binary vector pB7WGF2 providing an N-terminal GFP-tag using Gateway® technology (Invitrogen life sciences). For transient expression the construct was transformed into the *A. tumefacians* GV3101 strain under selection for spectinomycin, gentamycin and rifampicin.

mCherry-paGFP: Primer sequences are in supplemental table 1. For p35S::mCherry-paGFP-fABD2 primers were designed to amplify paGFP from the p35S::CXN-paGFP vector (Runions et al., 2006 [6]). The N-terminal FRD primer (JM393) was flanked with Gateway attB1 site and the C terminal REV primer (JM394) with a GGSGG amino acid linker overhang. fABD2 was then amplified by PCR using arabidopsis cDNA from five day old seedlings. The N-terminal FRD primer (JM395) consisted of a 22bp overhang composed of the GGSGG linker and last 7nt from paGFP. The C-terminal REV primer (JM392) contained a Gateway attB2 site. These DNA fragments were then fused together using the NEB HiFi Gibson assembly protocol. In order to generate p35S::mCherry-paGFP-Lifeact, paGFP fused to Lifeact was amplified from paGFP using an N-terminal primer (JM393), flanked with a Gateway attB1 site and a C-terminal REV primer (JM401) with an overhang composing a GGSGG linker, Lifeact and an attB2 site. Both constructs were then cloned into Gateway pDONR221 vector using BP clonase and subsequently a 35S promoter driven gateway compatible mCherry N-

397 terminal vector using LR clonase to give p35S::mCherry-paGFP-fABD2 and p35S::mCherry-
398 paGFP-Lifeact. These were then transformed into *A. tumefacians* GV3101 and selected for
399 with Spectinomycin (50µg/ml), Gentamycin 15 µg/ml and Rifampicin 25µg/ml.
400
401 *Live cell microscopy*
402 *Confocal:* Imaging was performed on Zeiss 880 or 800 confocal microscopes both equipped
403 with Airyscan detectors and 100X 1.46NA lenses. Samples were mounted on #1.5 coverslips
404 with dH_2O. Airyscan imaging was performed on the Zeiss 880 using a 5X digital zoom and a
405 500-550BP and 565LP dual emission filter. An additional 620SP filter was used to block
406 chlorophyll autofluorescence. For GFP and RFP/mCherry imaging, the 488 nm and 561 nm
407 lasers respectively were used for excitation and the frame integration time was 0.13s. For
408 GFP/RFP imaging, line switching was used (halving the frame rate). A minimum timeseries of
409 240 frames (≥30s) was collected for each FRAP and activation experiment. The FRAP
410 experimental sequence was five pre-bleach image scans followed by 10 bleaching scans with
411 the 488 nm laser at 100% in a square region (160x160 pixels) and then confocal imaging as
412 described above. For photoactivation experiments, the 405 nm laser was used at 50% power
413 for 10 iterations in a similarly square region to FRAP prior to imaging.
414 *TIRF:* TIRF imaging was performed on a Nikon Ti-E microscope equipped with an iLas2 TIRF
415 FRAP system (Roper), Triline laserbank (Cairn), HQ525/50m emission filter (Chroma) and
416 sCMOS detector (Prime 95B, Photometrics). A 100X 1.46NA lens was used and data was
417 collected using MetaMorph. Excitation and bleaching were performed with a 488nm laser,
418 with FRAP experiments involving 10 iterations of the 488nm laser at full power in the
419 selected region of interest (ROI).
420
421 *Image analysis*
422 Airyscan processing was performed in Zen Black version 2.1 SP3 14.0.0.0. ROI intensity data
423 was extracted using Zen blue (v2.3). Image editing, kymographs and temporal colour coded
424 projections was performed in FIJI (Image J version 1.51u). Golgi tracking was performed
425 using Trackmate (v3.6.0) [59]. The RFP channel was segmented using a LoG detector with an
426 estimated puncta diameter of 1µm, threshold of 10, a medium filter and sub-pixel
427 localisation. All Golgi bodies tracked for fewer than 5 frames were discarded. FRAP analysis
428 was performed as described in [60] with data being normalised and then fit to a non-linear
429 regression one phase association curve. Photoactivation intensity data was normalised in
430 the same way, however a non-linear regression one phase decay curve was fitted. For FRAP
431 and photoactivation data, as well as recovery / decay curves, $t_{1/2}$ and fluorescence plateau
432 values were calculated. In order to demonstrate actin sliding, the intensities in the
433 activation region and an adjacent region a set distance apart were analysed and normalised
434 to T0 = 100% fluorescence intensity.
435
436 ***Quantification and statistical analysis.***
437 Quantification of images was performed using either FIJI or Zen Blue. Data was collated in
438 Microsoft excel. For graph generation and statistical analysis Graphpad was used. For
439 reasons of clarity the statistical test performed (either ANOVA or t-test) and number of N for
440 each experiment is listed in the corresponding figure legend. Significant difference is defined
441 as: ns ≥ 0.05; * ≤ 0.05; ** ≤ 0.01; *** ≤ 0.001; **** ≤ 0.0001 and is indicated by asterisks
442 above each box-plot. For box plots, blue error bars indicate the standard deviation (SD) and
443 the red line represents mean value.

References

1. Ueda, H., Yokota, E., Kutsuna, N., Shimada, T., Tamura, K., Shimmen, T., Hasezawa, S., Dolja, V. V., and Hara-Nishimura, I. (2010). Myosin-dependent endoplasmic reticulum motility and F-actin organization in plant cells. Proc. Natl. Acad. Sci. *107*, 6894–6899. Available at: http://www.pnas.org/cgi/doi/10.1073/pnas.0911482107.
2. Boevink, P., Oparka, K., Santa Cruz, S., Martin, B., Betteridge, A., and Hawes, C. (1998). Stacks on tracks: the plant Golgi apparatus traffics on an actin/ER network. Plant J. *15*, 441–7. Available at: http://www.ncbi.nlm.nih.gov/pubmed/9750355.
3. Quader, H., Hofmann, A., and Schnepf, E. (1989). Reorganization of the endoplasmic reticulum in epidermal cells of onion bulb scales after cold stress: Involvement of cytoskeletal elements. Planta *177*, 273–280. Available at: https://doi.org/10.1007/BF00392816.
4. Saint-Jore, C.M., Evins, J., Batoko, H., Brandizzi, F., Moore, I., and Hawes, C. (2002). Redistribution of membrane proteins between the Golgi apparatus and endoplasmic reticulum in plants is reversible and not dependent on cytoskeletal networks. Plant J. *29*, 661–78. Available at: http://www.ncbi.nlm.nih.gov/pubmed/11874578.
5. Luis, L.P., Snapp, E.L., Lippincott-schwartz, J., Hawes, C., and Brandizzi, F. (2004). Endoplasmic Reticulum Export Sites and Golgi Bodies Behave as Single Mobile Secretory Units in Plant Cells. Plant Cell *16*, 1753–1771.
6. Runions, J., Brach, T., Kühner, S., and Hawes, C. (2006). Photoactivation of GFP reveals protein dynamics within the endoplasmic reticulum membrane. J. Exp. Bot. *57*, 43–50.
7. Sparkes, I., Runions, J., Hawes, C., and Griffing, L. (2009). Movement and Remodeling of the Endoplasmic Reticulum in Nondividing Cells of Tobacco Leaves. Plant Cell *21*, 3937–3949. Available at: http://www.plantcell.org/cgi/doi/10.1105/tpc.109.072249.
8. Griffing, L.R.R. (2010). Networking in the endoplasmic reticulum. Biochem. Soc. Trans. *38*, 747–753. Available at: http://biochemsoctrans.org/lookup/doi/10.1042/BST0380747.
9. Griffing, L.R., Lin, C., Perico, C., White, R.R., and Sparkes, I. (2017). Plant ER geometry and dynamics: biophysical and cytoskeletal control during growth and biotic response. Protoplasma *254*, 43–56. Available at: http://dx.doi.org/10.1007/s00709-016-0945-3.
10. Sheahan, M.B., Staiger, C.J., Rose, R.J., and McCurdy, D.W. (2004). A green fluorescent protein fusion to actin-binding domain 2 of Arabidopsis fimbrin highlights new features of a dynamic actin cytoskeleton in live plant cells. Plant Physiol. *136*, 3968–3978.
11. Staiger, C.J., Sheahan, M.B., Khurana, P., Wang, X., McCurdy, D.W., and Blanchoin, L. (2009). Actin filament dynamics are dominated by rapid growth and severing activity in the Arabidopsis cortical array. J. Cell Biol. *184*, 269–280.
12. Henty-Ridilla, J.L., Li, J., Blanchoin, L., and Staiger, C.J. (2013). Actin dynamics in the cortical array of plant cells. Curr. Opin. Plant Biol. *16*, 678–687. Available at: http://dx.doi.org/10.1016/j.pbi.2013.10.012.
13. Ryan, J.M., and Nebenführ, A. (2017). Update on Myosin Motors: Molecular Mechanisms and Physiological Functions. Plant Physiol. *176*, pp.01429.2017. Available at: http://www.plantphysiol.org/lookup/doi/10.1104/pp.17.01429.

491 14. Buchnik, L., Abu-Abied, M., and Sadot, E. (2015). Role of plant myosins in motile
492 organelles: Is a direct interaction required? J. Integr. Plant Biol. *57*, 23–30.
493 15. Higashi-Fujime, S., Ishikawa, R., Iwasawa, H., Kagami, O., Kurimoto, E., Kohama, K.,
494 and Hozumi, T. (1995). The fastest actin-based motor protein from the green algae,
495 Chara, and its distinct mode of interaction with actin. FEBS Lett. *375*, 151–4. Available
496 at: http://www.ncbi.nlm.nih.gov/pubmed/7498467.
497 16. Yamamoto, K., Kikuyama, M., Sutoh-Yamamoto, N., and Kamitsubo, E. (1994).
498 Purification of Actin Based Motor Protein from Chara corallina. Proc. Japan Acad. Ser.
499 B Phys. Biol. Sci. *70*, 175–180. Available at:
500 http://joi.jlc.jst.go.jp/JST.Journalarchive/pjab1977/70.175?from=CrossRef.
501 17. Mehta, A.D., Rock, R.S., Rief, M., Spudich, J.A., Mooseker, M.S., and Cheney, R.E.
502 (1999). Myosin-V is a processive actin-based motor. Nature *400*, 590–3. Available at:
503 http://dx.doi.org/10.1038/23072.
504 18. Tominaga, M., and Nakano, A. (2012). Plant-Specific Myosin XI, a Molecular
505 Perspective. Front. Plant Sci. *3*, 1–11. Available at:
506 http://journal.frontiersin.org/article/10.3389/fpls.2012.00211/abstract.
507 19. Peremyslov, V. V., Prokhnevsky, A.I., and Dolja, V. V. (2010). Class XI Myosins Are
508 Required for Development, Cell Expansion, and F-Actin Organization in *Arabidopsis*.
509 Plant Cell *22*, 1883–1897. Available at:
510 http://www.plantcell.org/lookup/doi/10.1105/tpc.110.076315.
511 20. Cai, C., Henty-Ridilla, J.L., Szymanski, D.B., and Staiger, C.J. (2014). Arabidopsis myosin
512 XI: a motor rules the tracks. Plant Physiol. *166*, 1359–70. Available at:
513 http://www.pubmedcentral.nih.gov/articlerender.fcgi?artid=4226357&tool=pmcentr
514 ez&rendertype=abstract.
515 21. Tominaga, M., Kimura, A., Yokota, E., Haraguchi, T., Shimmen, T., Yamamoto, K.,
516 Nakano, A., and Ito, K. (2013). Cytoplasmic Streaming Velocity as a Plant Size
517 Determinant. Dev. Cell *27*, 345–352. Available at:
518 http://dx.doi.org/10.1016/j.devcel.2013.10.005.
519 22. Li, X.D., Hyun, S.J., Mabuchi, K., Craig, R., and Ikebe, M. (2006). The globular tail
520 domain of myosin Va Functions as an inhibitor of the myosin Va motor. J. Biol. Chem.
521 *281*, 21789–21798.
522 23. Kriechbaumer, V., Botchway, S.W., Slade, S.E., Knox, K., Frigerio, L., Oparka, K., and
523 Hawes, C. (2015). Reticulomics: Protein-Protein Interaction Studies with Two
524 Plasmodesmata-Localized Reticulon Family Proteins Identify Binding Partners
525 Enriched at Plasmodesmata, Endoplasmic Reticulum, and the Plasma Membrane.
526 Plant Physiol. *169*, 1933–45. Available at:
527 http://www.plantphysiol.org/lookup/doi/10.1104/pp.15.01153.
528 24. Peremyslov, V. V, Klocko, A.L., Fowler, J.E., and Dolja, V. V (2012). Arabidopsis myosin
529 XI-K localizes to the motile endomembrane vesicles associated with F-actin. *3*, 1–10.
530 25. Sattarzadeh, A., Schmelzer, E., and Hanson, M.R. (2011). Analysis of Organelle
531 Targeting by DIL Domains of the Arabidopsis Myosin XI Family. Front. Plant Sci. *2*, 1–
532 11. Available at:
533 http://journal.frontiersin.org/article/10.3389/fpls.2011.00072/abstract.
534 26. Sparkes, I.A., Teanby, N.A., and Hawes, C. (2008). Truncated myosin XI tail fusions
535 inhibit peroxisome, Golgi, and mitochondrial movement in tobacco leaf epidermal
536 cells: A genetic tool for the next generation. J. Exp. Bot. *59*, 2499–2512.
537 27. Okamoto, M., Kurokawa, K., Matsuura-Tokita, K., Saito, C., Hirata, R., and Nakano, A.

538 (2012). High-curvature domains of the ER are important for the organization of ER
539 exit sites in Saccharomyces cerevisiae. J. Cell Sci. *125*, 3412–3420. Available at:
540 http://jcs.biologists.org/cgi/doi/10.1242/jcs.100065.
541 28. Hawes, C., Kiviniemi, P., and Kriechbaumer, V. (2015). The endoplasmic reticulum: A
542 dynamic and well-connected organelle. J. Integr. Plant Biol. *57*, 50–62.
543 29. Latijnhouwers, M., Gillespie, T., Boevink, P., Kriechbaumer, V., Hawes, C., and
544 Carvalho, C.M. (2007). Localization and domain characterization of Arabidopsis golgin
545 candidates. J. Exp. Bot. *58*, 4373–4386.
546 30. OSTERRIEDER, A. (2012). Tales of tethers and tentacles: golgins in plants. J. Microsc.
547 *247*, 68–77. Available at: https://doi.org/10.1111/j.1365-2818.2012.03620.x.
548 31. Stefano, G., and Brandizzi, F. (2017). Advances in plant ER architecture and dynamics.
549 Plant Physiol. *176*, pp.01261.2017. Available at:
550 http://www.plantphysiol.org/lookup/doi/10.1104/pp.17.01261.
551 32. Cao, P., Renna, L., Stefano, G., and Brandizzi, F. (2016). SYP73 Anchors the ER to the
552 Actin Cytoskeleton for Maintenance of ER Integrity and Streaming in Arabidopsis.
553 Curr. Biol. *26*, 3245–3254. Available at: http://dx.doi.org/10.1016/j.cub.2016.10.024.
554 33. Lerich, A., Hillmer, S., Langhans, M., Scheuring, D., van Bentum, P., and Robinson,
555 D.G. (2012). ER Import Sites and Their Relationship to ER Exit Sites: A New Model for
556 Bidirectional ER-Golgi Transport in Higher Plants. Front. Plant Sci. *3*, 1–21. Available
557 at: http://journal.frontiersin.org/article/10.3389/fpls.2012.00143/abstract.
558 34. Wang, P., and Hussey, P.J. (2017). NETWORKED 3B: A novel protein in the actin
559 cytoskeleton-endoplasmic reticulum interaction. J. Exp. Bot. *68*, 1441–1450.
560 35. Ketelaar, T., Allwood, E.G., Anthony, R., Voigt, B., Menzel, D., and Hussey, P.J. (2004).
561 The Actin-Interacting Protein AIP1 Is Essential for Actin Organization and Plant
562 Development. Curr. Biol. *14*, 145–149.
563 36. Smertenko, A.P., Deeks, M.J., and Hussey, P.J. (2010). Strategies of actin
564 reorganisation in plant cells. J. Cell Sci. *123*, 3029–3029. Available at:
565 http://jcs.biologists.org/cgi/doi/10.1242/jcs.079749.
566 37. Riedl, J., Crevenna, A.H., Kessenbrock, K., Yu, J.H., Neukirchen, D., Bista, M., Bradke,
567 F., Jenne, D., Holak, T. a, Werb, Z., *et al.* (2008). Lifeact: a versatile marker to visualize
568 F-actin. Nat. Methods *5*, 605–7. Available at:
569 http://www.ncbi.nlm.nih.gov/pubmed/18536722.
570 38. Rocchetti, A., Hawes, C., Kriechbaumer, V., Hamers-Casterman, C., Atarhouch, T.,
571 Muyldermans, S., Robinson, G., Hamers, C., Songa, E., Bendahman, N., *et al.* (2014).
572 Fluorescent labelling of the actin cytoskeleton in plants using a cameloid antibody.
573 Plant Methods *10*, 12. Available at:
574 http://plantmethods.biomedcentral.com/articles/10.1186/1746-4811-10-12.
575 39. Avisar, D., Abu-Abied, M., Belausov, E., Sadot, E., Hawes, C., and Sparkes, I.A. (2009).
576 A Comparative Study of the Involvement of 17 Arabidopsis Myosin Family Members
577 on the Motility of Golgi and Other Organelles. Plant Physiol. *150*, 700–709. Available
578 at: http://www.plantphysiol.org/cgi/doi/10.1104/pp.109.136853.
579 40. McCurdy, D.W. (1999). Is 2,3-butanedione monoxime an effective inhibitor of myosin-
580 based activities in plant cells? Protoplasma *209*, 120–5. Available at:
581 http://www.ncbi.nlm.nih.gov/pubmed/18987800.
582 41. Seki, M., Awata, J.Y., Shimada, K., Kashiyama, T., Ito, K., and Yamamoto, K. (2003).
583 Susceptibility of Chara myosin to SH reagents. Plant Cell Physiol. *44*, 201–205.
584 42. Griffing, L.R., Gao, H.T., and Sparkes, I. (2014). ER network dynamics are differentially

585 controlled by myosins XI-K, XI-C, XI-E, XI-I, XI-1, and XI-2. Front. Plant Sci. *5*, 1–12.
586 Available at: http://journal.frontiersin.org/article/10.3389/fpls.2014.00218/abstract.
587 43. Mathur, J., Spielhofer, P., Kost, B., and Chua, N. (1999). The actin cytoskeleton is
588 required to elaborate and maintain spatial patterning during trichome cell
589 morphogenesis in Arabidopsis thaliana. Development *126*, 5559–5568. Available at:
590 http://www.ncbi.nlm.nih.gov/entrez/query.fcgi?db=pubmed&cmd=Retrieve&a
591 mp;dopt=AbstractPlus&list_uids=10572033%5Cnhttp://www.ncbi.nlm.nih.gov/e
592 ntrez/query.fcgi?db=pubmed&cmd=Retrieve&dopt=AbstractPlus&list_uids=1057203
593 3%5Cnpapers2://publication/uui.
594 44. Sampathkumar, A., Lindeboom, J.J., Debolt, S., Gutierrez, R., Ehrhardt, D.W., Ketelaar,
595 T., and Persson, S. (2011). Live Cell Imaging Reveals Structural Associations between
596 the Actin and Microtubule Cytoskeleton in Arabidopsis. Plant Cell *23*, 2302–2313.
597 Available at:
598 http://www.pubmedcentral.nih.gov/articlerender.fcgi?artid=3160026&tool=pmcentr
599 ez&rendertype=abstract%5Cnhttp://www.plantcell.org/lookup/doi/10.1105/tpc.111.
600 087940.
601 45. Bubb, M.R., Spector, I., Beyer, B.B., and Fosen, K.M. (2000). Effects of jasplakinolide
602 on the kinetics of actin polymerization. An explanation for certain in vivo
603 observations. J. Biol. Chem. *275*, 5163–5170.
604 46. Bubb, M.R., Senderowicz, A.M.J., Sausville, E.A., Duncan, K.L.K., and Korn, E.D. (1994).
605 Jasplakinolide, a cytotoxic natural product, induces actin polymerization and
606 competitively inhibits the binding of phalloidin to F-actin. J. Biol. Chem. *269*, 14869–
607 14871.
608 47. Peremyslov, V. V., Prokhnevsky, A.I., Avisar, D., and Dolja, V. V. (2008). Two class XI
609 myosins function in organelle trafficking and root hair development in Arabidopsis.
610 Plant Physiol. *146*, 1109–16. Available at:
611 http://www.plantphysiol.org/cgi/doi/10.1104/pp.107.113654.
612 48. Satiat-Jeunemaitre, B., Steele, C., and Hawes, C. (1996). Golgi-membrane dynamics
613 are cytoskeleton dependent: A study on Golgi stack movement induced by brefeldin
614 A. Protoplasma *191*, 21–33. Available at: https://doi.org/10.1007/BF01280822.
615 49. Nebenführ, A., Gallagher, L.A., Dunahay, T.G., Frohlick, J.A., Mazurkiewicz, A.M.,
616 Meehl, J.B., and Staehelin, L.A. (1999). Stop-and-go movements of plant Golgi stacks
617 are mediated by the acto-myosin system. Plant Physiol. *121*, 1127–42. Available at:
618 http://www.plantphysiol.org/lookup/doi/10.1104/pp.121.4.1127.
619 50. Osterrieder, A., Sparkes, I.A., Botchway, S.W., Ward, A., Ketelaar, T., de Ruijter, N.,
620 and Hawes, C. (2017). Stacks off tracks: a role for the golgin AtCASP in plant
621 endoplasmic reticulum-Golgi apparatus tethering. J. Exp. Bot. *68*, 3339–3350.
622 Available at: http://www.ncbi.nlm.nih.gov/pubmed/28605454.
623 51. daSilva, L.L.P., Snapp, E.L., Denecke, J., Lippincott-Schwartz, J., Hawes, C., and
624 Brandizzi, F. (2004). Endoplasmic reticulum export sites and Golgi bodies behave as
625 single mobile secretory units in plant cells. Plant Cell *16*, 1753–71. Available at:
626 http://www.plantcell.org/cgi/doi/10.1105/tpc.022673.
627 52. Avisar, D., Prokhnevsky, A.I., Makarova, K.S., Koonin, E. V., and Dolja, V. V. (2008).
628 Myosin XI-K Is Required for Rapid Trafficking of Golgi Stacks, Peroxisomes, and
629 Mitochondria in Leaf Cells of Nicotiana benthamiana. Plant Physiol. *146*, 1098–1108.
630 Available at: http://www.plantphysiol.org/cgi/doi/10.1104/pp.107.113647.
631 53. van der Honing, H.S., van Bezouwen, L.S., Emons, A.M.C., and Ketelaar, T. (2011). High

632 expression of Lifeact in Arabidopsis thaliana reduces dynamic reorganization of actin
633 filaments but does not affect plant development. Cytoskeleton *68*, 578–587.
634 54. Wang, P., Hawkins, T.J., Richardson, C., Cummins, I., Deeks, M.J., Sparkes, I., Hawes,
635 C., and Hussey, P.J. (2014). The plant cytoskeleton, NET3C, and VAP27 mediate the
636 link between the plasma membrane and endoplasmic reticulum. Curr. Biol. *24*, 1397–
637 1405.
638 55. Tokuo, H., Mabuchi, K., and Ikebe, M. (2007). The motor activity of myosin-X
639 promotes actin fiber convergence at the cell periphery to initiate filopodia formation.
640 J. Cell Biol. *179*, 229–238.
641 56. Joensuu, M., Belevich, I., Ramo, O., Nevzorov, I., Vihinen, H., Puhka, M., Witkos, T.M.,
642 Lowe, M., Vartiainen, M.K., and Jokitalo, E. (2014). ER sheet persistence is coupled to
643 myosin 1c-regulated dynamic actin filament arrays. Mol. Biol. Cell *25*, 1111–1126.
644 Available at: http://www.molbiolcell.org/cgi/doi/10.1091/mbc.E13-12-0712.
645 57. Van Der Honing, H.S., De Ruijter, N.C.A., Mie, A., Emons, C., and Ketelaar, T. (2010).
646 Actin and myosin regulate cytoplasm stiffness in plant cells: a study using optical
647 tweezers. New Phytol. *185*, 90–102.
648 58. Sparkes, I.A., Runions, J., Kearns, A., and Hawes, C. (2006). c. Nat. Protoc. *1*, 2019.
649 Available at: http://dx.doi.org/10.1038/nprot.2006.286.
650 59. Tinevez, J.Y., Perry, N., Schindelin, J., Hoopes, G.M., Reynolds, G.D., Laplantine, E.,
651 Bednarek, S.Y., Shorte, S.L., and Eliceiri, K.W. (2017). TrackMate: An open and
652 extensible platform for single-particle tracking. Methods *115*, 80–90. Available at:
653 http://dx.doi.org/10.1016/j.ymeth.2016.09.016.
654 60. Martinière, A., Lavagi, I., Nageswaran, G., Rolfe, D.J., Maneta-Peyret, L., Luu, D.-T.,
655 Botchway, S.W., Webb, S.E.D., Mongrand, S., Maurel, C., *et al.* (2012). Cell wall
656 constrains lateral diffusion of plant plasma-membrane proteins. Proc. Natl. Acad. Sci.
657 U. S. A. *109*, 12805–10. Available at:
658 http://www.pubmedcentral.nih.gov/articlerender.fcgi?artid=3411962&tool=pmcentr
659 ez&rendertype=abstract [Accessed September 8, 2014].
660
661
662
663
664